Inkjet-Printed Line Morphologies and Temperature Control of the Coffee Ring Effect

ARTICLE *in* LANGMUIR · APRIL 2008

Impact Factor: 4.46 · DOI: 10.1021/la7026847 · Source: PubMed

2 AUTHORS, INCLUDING:

Vivek Subramanian
University of California, Berkeley
87 PUBLICATIONS **1,926** CITATIONS

SEE PROFILE

Inkjet-Printed Line Morphologies and Temperature Control of the Coffee Ring Effect

Dan Soltman* and Vivek Subramanian

Department of Electrical Engineering and Computer Science, University of California, Berkeley, California 94720

Received August 30, 2007. In Final Form: October 17, 2007

We have studied inkjet-printed drops of a conductive polymer. We show how varying drop spacing and temperature lead to several different printed line morphologies and offer a simple geometric explanation for these various forms. Also, by controlling the evaporation profile of drying drops and lines, we demonstrate control of the coffee ring effect by which solute is transferred to the rim. Under appropriate conditions, we are able to enhance or eliminate the coffee ring effect in our drying features.

1. Introduction

Solution-processable electronics have attracted considerable attention and research. They combine simple additive processing with novel low-cost materials and have the potential to drastically lower the cost of integrated circuit fabrication, especially compared to that for conventional silicon processing. Inkjet printing, one solution processing technique, has been demonstrated to be able to print all materials required for integrated circuits: conductors, semiconductors, and dielectrics, and thus transistors.[1] When combined with other solution processing techniques, such as roll-to-roll gravure printing, one can imagine drastically reducing the cost of circuits in applications such as RFID chips and displays

For integrated circuits, ideal inkjet-printed lines would be smooth, even, narrow, and straight. However, recent work from our group and others demonstrates a need for improved control of the behavior of inkjet-printed inks.[2,3] Representative images of inkjet-printed features from each paper are included in Figure 1. In both cases, we see that in order to create a straight, predictable line smoothness and evenness were sacrificed.

In printed integrated electronics, the various roles of electrically active material lead to different engineering constraints. For example, in a bottom-gated transistor, the gate line must be as narrow and as smooth as possible. The source and drain need smooth edges with a small, controlled separation although their width is less critical. For a high-*Q* inductor or interconnecting wire, pitch and conductivity are more important than smoothness or edge uniformity. Finally, for organic LEDs, smoothness and film uniformity are paramount to achieving uniform emission. By characterizing and understanding the conditions that lead to different printed line morphologies, this article seeks to advance the control and optimization of inkjet-printed lines, especially in electronics applications.

This work builds most directly upon the work of Duineveld, who also identified printed line phenomena and quantified the conditions leading to them.[5] Our work will extend the discussion of the morphologies and the conditions leading to them. We will help to classify and understand the conditions that lead to a uniform printed line such as that shown by Perelaer et al.[6] Like de Gans and Schubert, we will discuss the tendency of evaporating solvents to leave behind coffee rings.[7] Unlike dual solvent systems that they and others demonstrate, we will show how one can control and reverse the coffee ring effect via substrate temperature in a single-solvent system.[8] Researchers have also eliminated coffee rings in printed features using a thermally gelating ink on a heated substrate.[9] Finally, our work will offer counter evidence to a theoretical result that coffee ring features are enhanced when evaporation is decreased.[10]

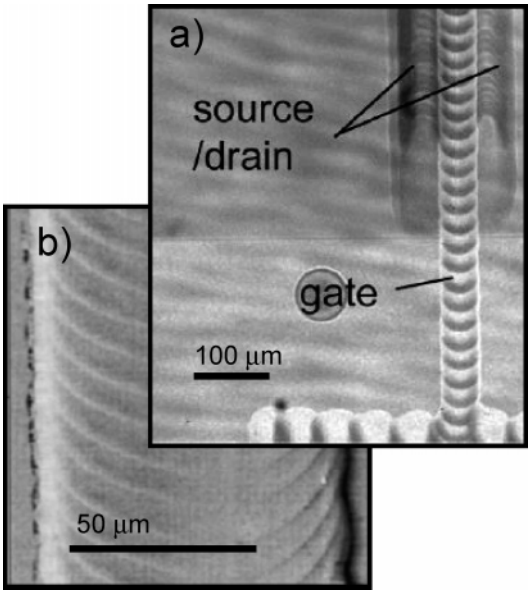

Figure 1. (a) Micrograph of inkjet-printed TFT with pedot contacts[4] and (b) AFM of an inkjet-printed gold nanoparticle line.[2]

* Corresponding author. E-mail: soltman@eecs.berkeley.edu.

(1) Subramanian, V.; Chang, P. C.; Lee, J. B.; Molesa, S. E.; Volkman, S. K. *IEEE Trans. Compon. Packag. Technol.* **2005**, *28*, 742−747.

(2) Huang, D.; Liao, F.; Molesa, S.; Redinger, D.; Subramanian, V. *J. Electrochem. Soc.* **2003**, *150*, G412−G417.

(3) Kawase, T.; Shimoda, T.; Newsome, C.; Sirringhaus, H.; Friend, R. H. *Thin Solid Films* **2003**, *438*, 279−287.

(4) Burns, S. E.; Cain, P.; Mills, J.; Wang, J. Z.; Sirringhaus, H. *MRS Bull.* **2003**, *28*, 829−834.

(5) Duineveld, P. C. *J. Fluid Mech.* **2003**, *477*, 175−200.

(6) Perelaer, J.; de Gans, B. J.; Schubert, U. S. *Adv. Mater.* 2006, *18*, 2101−2104.

(7) de Gans, B. J.; Schubert, U. S. *Langmuir* **2004**, *20*, 7789−7793.

(8) Park, J.; Moon, J. *Langmuir* **2006**, *22*, 3506−3513.

(9) van den Berg, A. M. J.; de Laat, A. W. M.; Smith, P. J.; Perelaer, J.; Schubert, U. S. *J. Mater. Chem.* **2007**, *17*, 677−683.

(10) Ozawa, K.; Nishitani, E.; Doi, M. *Jpn. J. Appl. Phys., Part 1* **2005**, *44*, 4229−4234.

10.1021/la7026847 CCC: $40.75
Published on Web 01/16/2008 PAGE EST: 7.9

2. Experiment

We carry out our experiments on a custom-built research inkjet printer. We use Microfab piezoelectric drop-on-demand dispensing heads with a 60 μm orifice. Our stages have *x*, *y*, and rotational degrees of freedom with 1 μm accuracy. Operating in drop-on-demand mode, our printer has a base drop frequency of approximately 30 Hz, with the option to delay dropping further. Falling drops have a diameter similar to that of the dispensing head orifice and a volume of approximately 100 pL and eject at 1 to 2 m/s, though there is significant variation due to ink, atmospheric, and substrate conditions.

The ink used throughout this experiment is poly(3,4-ethylenedioxythiophene) poly(styrenesulfonate), PEDOT/PSS 1.3% by weight in water from Aldrich, referred to as pedot hereafter. It is a common conductive polymer used for organic LEDs and as an antistatic coating. We printed onto 5 cm × 7 cm glass slides coated with spun poly(4-vinylphenol) dielectric, PVP, thermally cross linked at 200 °C. Because we commonly use PVP both as a smoothing layer on low-cost plastic and a thin printable dielectric, the PVP insured that our results will be transferable to low-cost substrates.[11] AFM profiling reveals the PVP film to be exceptionally smooth, with an rms roughness of 3.34 Å. The static contact angle of pedot on the PVP-coated glass is 82.7 ± 1.7°, as extracted from a sessile drop by a Kruss contact angle measuring system. We assume that this approximates the advancing contact angle. Under no conditions do we observe the contact line to retreat, and thus we assume zero retreating contact angle as others have seen when working with aqueous pedot ink.[5]

The independent variables used in this experiment are substrate temperature, drop spacing, and drop frequency. The PVP-coated glass substrate and pedot ink remain constant. The substrate is cooled to 17 °C via a cooling water line and heated to as warm as 60 °C. Drop spacing varies from 5 to 100 μm center-to-center. At low spacing, an overflowing irregular bead forms, and isolated drops land at large spacing. (Note that we refer to a printed bead when wet and to a printed line when dry.) Finally, as mentioned above, the minimum drop-on-demand delay is about 30 ms on our printer. Delays from 10 to 2000 ms are appended, though on the 1 s time scale clogging becomes a problem because the ink has sufficient time to form a skin at the nozzle. Misdirected drops and/or clogs often result from delays of 1000 to 2000 ms; this limit places an upper limit on delay for low-temperature substrates. Once printed, the resulting patterns are measured and quantified with a variety of tools, especially an optical microscope and a mechanical stylus profilometer.

3. Results

A few principal behaviors emerge when examining printed pedot patterns across a variety of drop spacings, delay periods, and temperatures. We label these as individual drops, a scalloped line, a uniform line, a bulging line, and stacked coins. Figure 2 shows these five basic morphologies.

If one prints drops that are too far apart to interact, more than twice a drop's radius, then isolated drops land and dry. Individual drops occur at drop spacings above about 100 μm independent of temperature or delay in our system.

At lower temperature, as drop spacing decreases, isolated drops overlap and merge but retain individual rounded contact lines, and a scalloped pattern emerges. These scalloped lines are narrower than an isolated drop as fluid expansion is partially arrested.

Further decreasing the drop spacing will eliminate the scalloping and lead to a smooth, straight line. These lines have a uniform smooth edge and top. They are the narrowest lines printed.

(11) Molesa, S. E.; de la Fuente Vornbrock, A.; Chang, P. C.; Subramanian, V. Low-Voltage Inkjetted Organic Transistors for Printed RFID and Display Applications. In *Electron Devices Meeting*; IEEE International: 2005; Vol. IEDM Technical Digest, pp 109−112.

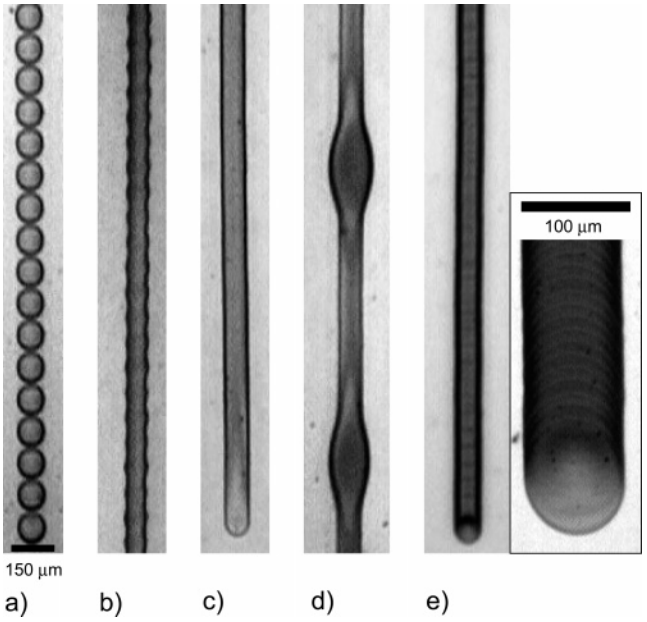

Figure 2. Examples of principal printed line behaviors: (a) individual drops, (b) scalloped, (c) uniform, (d) bulging, and (e) stacked coins. Drop spacing decreases from left to right.

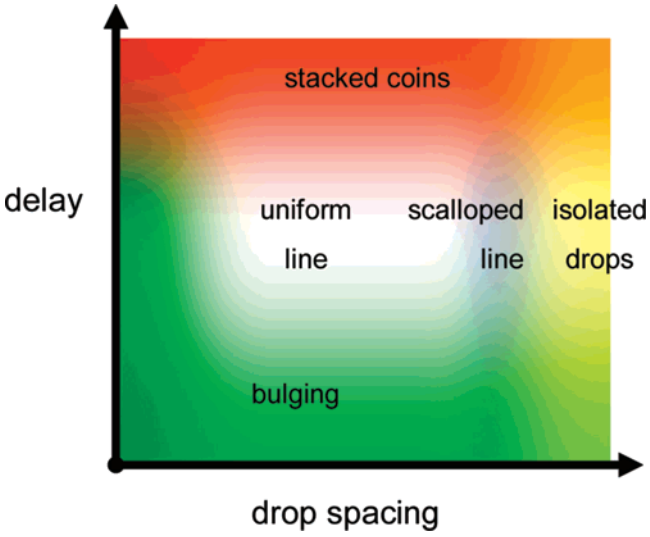

Figure 3. Typical printed line behavior at an intermediate temperature.

Printing drops even closer together leads to discreet bulging along the line's length, separated by regions of uniform narrow lines. These bulges tend to form periodically and also at the beginning of the line. Duineveld gives this striking behavior excellent consideration. Essentially, additional fluid from printing exceeds a bead's equilibrium contact angle, and discreet regions of outflow result, leading to rounded bulges in the dried feature.[5]

If the substrate temperature increases such that the evaporation time of a single drop is less than the drop jetting period, then each landing drop will dry individually regardless of overlap, leading to what looks like offset stacked coins (as also shown in Figure 1). At a given substrate temperature, increasing the drop delay will affect the onset of the stacked coin behavior. Drop spacing has no effect on the width of the lines printed in this regime because each drop dries individually. Figure 3 schematically shows where each of these behaviors tends to be found relative to one another at an intermediate temperature.

By carefully optimizing the drop frequency, temperature, and spacing, it is possible to print a smooth, narrow line with an even

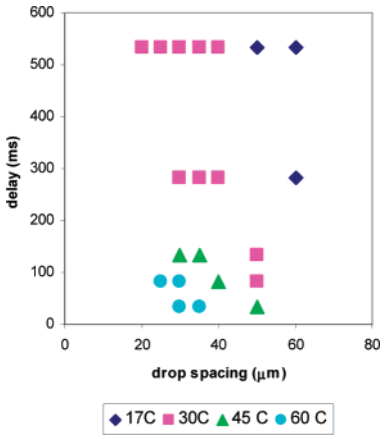

Figure 4. Experimental space leading to a uniform line, 17−60 °C.

edge. Qualitatively, the ideal line avoids bulging by slowing down the drop frequency until the advancing contact angle is never exceeded but is not so slow that drops dry within the period of one or two drops landing, avoiding stacked coins. It has a low enough drop spacing to avoid scalloping, and the delay is not so slow that the dropping frequency is comparable to the time it takes for the orifice to form a skin, thereby avoiding unpredictable drop trajectories. Figure 4 shows the experimental conditions where this good profile is found for practical temperatures from 17 to 60 °C. As expected, acceptable delay and spacing decreases occur at higher temperature. In fact, at 45 °C and above uniform lines could be printed at the native frequency of our printer. At temperatures above 60 °C, it is increasingly difficult to print uniform lines because the stacked coin behavior occurs at lower dropping frequency and solvent evaporation at the inkjet head leads to reliability issues.

A second effect, which is important to the quality and utility of the printed line, is seen by comparing the cross sections of these ideal lines across the range of temperatures. Figure 5 shows traces across uniform lines taken by a mechanical stylus profiler (Alpha-Step IQ surface profiler). Whereas the profile is smooth and convex at low temperature, it becomes increasingly concave at higher temperature. Indeed, at room temperature (30 °C) this transition toward a concave profile is a squared cross section. Interestingly, this temperature-dependent coffee ring control is valid for any of the above five principal line behaviors. One can tune the relative distribution of material across the printed line by controlling the drop temperature for any of the five line behaviors, which is a useful result for printing.

4. Temperature Control of Coffee Rings

The coffee ring deposits left by evaporating drops with pinned contact lines was first explained by Deegan et al.[12] He showed that a flux of fluid to the edge of the drop led to the buildup of solute there as the drop evaporated. Both the geometric nature of pinning and the increased evaporation due to curvature at the drop's edge contribute to the strength of the coffee ring. By drawing an analogy to an equivalent electrostatic problem, he is able to adopt the result of a previously solved geometry.

At room temperature, we are able to explain the presence of coffee rings in our lines (Figure 5) and drops (Figure 6) by utilizing Deegan's explanation. However, with a heated or cooled substrate, our evaporating features are now subject to a heat flux from the surface, breaking the symmetry that permitted Deegan's exact solution. In our evaporating drops and lines, heat is readily transferred from the substrate to the thin pinned edge of the drop, leading to enhanced evaporation near the drop's edge compared to that at the center. Pedot moves to the drop's edge to replace fluid lost to evaporation. Increasing the substrate temperature increases the size of this solute transfer toward the contact line. In the case of cooling, decreased rim evaporation eliminates coffee ring formation altogether because the cooled substrate retards edge evaporation more than that in the center.

Comparing the line and drop cross sections, we see that the effect of temperature on coffee ring formation is enhanced in drops. Table 1 below shows that the peak-to-valley coffee ring factor is larger for a drop when compared to that for a uniform line printed at the same temperature. This corroborates the contact line evaporation explanation. Compared to a uniform line, a circular drop has a greater ratio of edge length to interior area. Hence, the drop shows a greater transfer of solute to its edge when subjected to heating.

Our explanation of the effect of temperature on coffee ring deposits does not require a consideration of the temperature dependence of surface tension. However, published research on the coffee ring effect warrants a discussion of surface tension-driven flow, known as the Marangoni effect. Previous work has shown that the coffee ring effect can be controlled or eliminated through engineering an appropriate Marangoni flow.[7] Hu and Larson show that Marangoni flows in an evaporating octane drop lead to a deposition of solute at its center rather than a coffee ring at its perimeter.[13] However, in the same letter they found no such effect in an evaporating water droplet, even when avoiding surfactant contamination. Other work by Savino et al. presented a similar conclusion, witnessing Marangoni flows in drops of evaporating organic solvent but not water.[14] Therefore, in our work, where water is used as a solvent for pedot and is subjected to a significant delivery pathway (reservoir, tubing, ink-jet head), there is no reason to suspect that our drops have Marangoni flow. In fact, enhanced coffee rings at higher temperature, as we observed, are contrary to temperature-driven Marangoni flows that would increasingly redistribute pedot solute to a feature's center on warmer substrates.

5. Geometric Explanation of Principle Printed Line Behaviors

Expanding upon the qualitative explanation of printed bead topology discussed earlier, dimensional analysis and some geometry lead to more satisfying explanations for many of the line topologies noted above in Figure 2. These behaviors, illustrated in greater detail in Figure 7, occur across a broad range of temperatures. As we increase the drop spacing above a certain length, we observe that the resultant contact line changes from a smooth line (Figure 7a) to a rounded "scalloped" one (Figure 7b) and then eventually separates into isolated drops (Figure 7d). The paired drops of Figure 7c will be discussed below. Drop spacings are given in terms of physical radius and dimensionless radius, y, the ratio of drop spacing to landed drop radius. As we will show, much of the printed line behavior can be explained through this dimensionless quantity.

(12) Deegan, R. D.; Bakajin, O.; Dupont, T. F.; Huber, G.; Nagel, S. R.; Witten, T. A. *Nature* **1997**, *389*, 827−829.

(13) Hu, H.; Larson, R. G. *J. Phys. Chem. B* **2006**, *110*, 7090−7094.

(14) Savino, R.; Paterna, D.; Favaloro, N. *J. Thermophys. Heat Trans.* **2002**, *16*, 562−574.

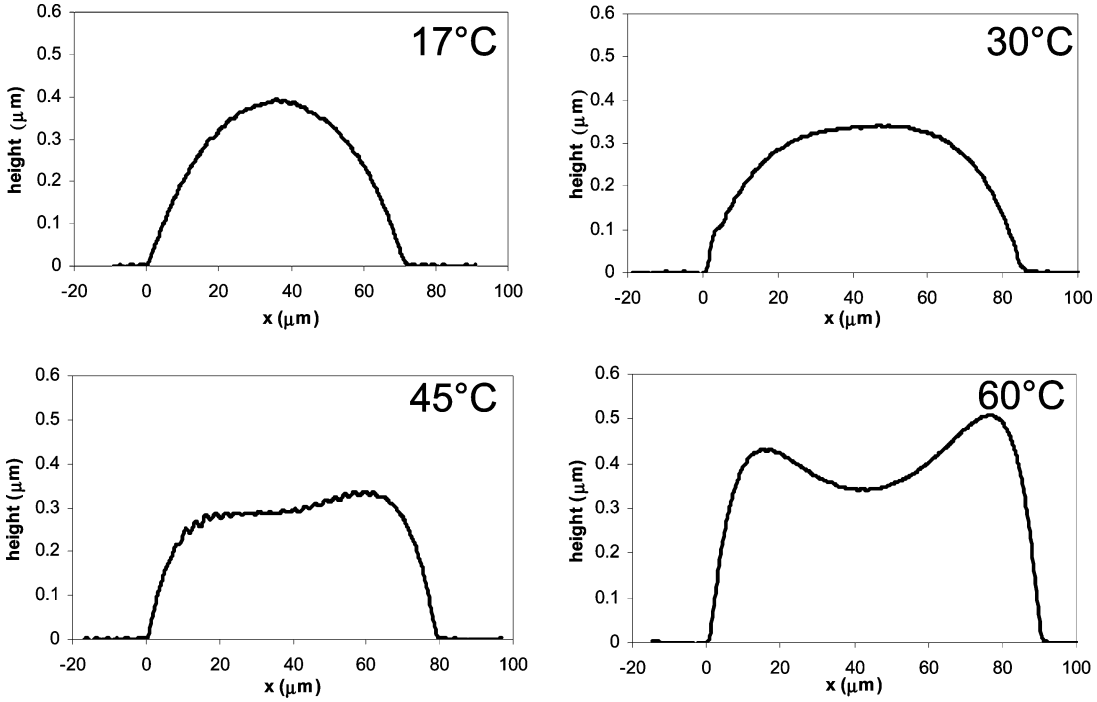

Figure 5. Cross-sectional profile of uniform lines printed at the noted temperature using a mechanical stylus profiler. (The delay and spacing are adjusted to be appropriate for each temperature.)

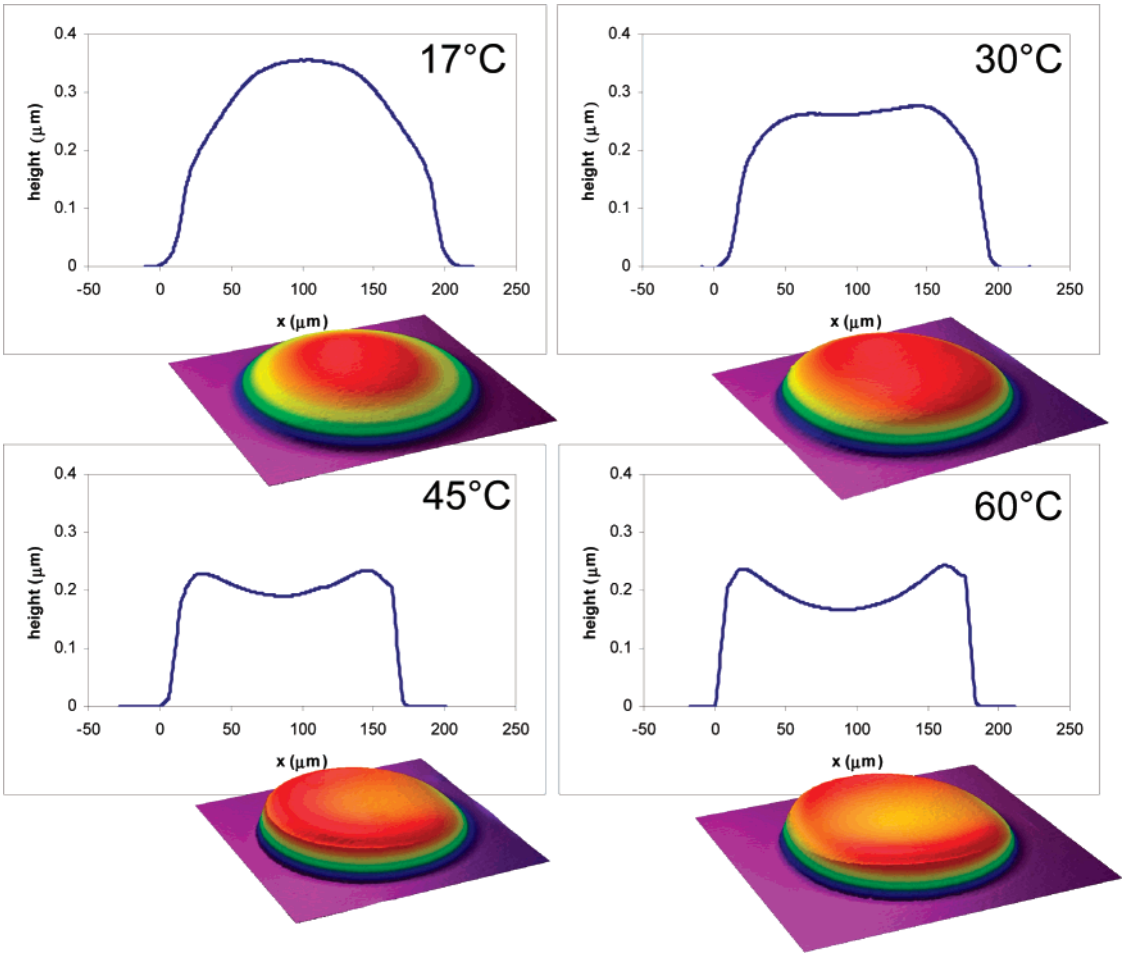

Figure 6. Cross section and 3D projection from an optical profilometer of single drops printed at the noted temperatures.

A simple 2D model of an expanding drop impinging upon the already formed, wetted bead explains these results succinctly. We will consider only the contact line of the uniform bead and that of the nearby next drop.

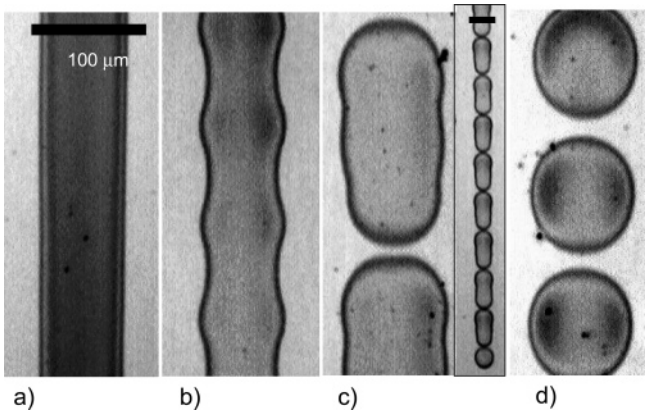

Figure 7. Printed line behaviors near the scallop transition (all line printed at 45 °C): (a) uniform line, drop spacing is 50 μm, $y = 1.10$; (b) scalloped line, drop spacing is 75 μm, $y = 1.65$; (c) pairs, drop spacing is 88 μm, $y = 1.84$ (with a low-magnification inset); and (d) isolated drops, drop spacing is 100 μm, $y = 2.20$.

To develop this model, first we must consider the volume of fluid being deposited per unit length. This is found from the drop volume (V_{drop}) and drop spacing (Δx) on the substrate.

$$\frac{\text{volume}}{\text{unit length}} = \frac{V_{drop}}{\Delta x} \tag{1}$$

Assuming that these drops will reflow into a cylindrical bead with the equilibrium contact angle, we can find the radius, R_1, of an equivalent-volume cylinder. Because the Bond number of the system is on the order of 10^{-3}, we use a cylindrical cap for the cylindrical bead (and a spherical cap for an isolated drop). Figure 8a shows the relevant geometry. The empirically determined contact angle of this system is 82.7°, which we assume will set the width of the cylindrical line.

Equating the fluid volume per unit length of landing drops to that of a half-cylinder, we introduce a contact angle factor $f(\theta)$ to correct the cross-sectional area of the half-cylinder bead appropriately from its ideal circular cross section (with a 90° contact angle). We use this correction factor to keep the equations from appearing overly complex because the contact angle remains fixed for the system. Rewriting this expression in terms of R_1 proves useful later in the analysis.

$$\frac{V_{drop}}{\Delta x} = \frac{1}{2}\pi {R_1}^2 f(\theta)$$

$$R_1 = \sqrt{\frac{2V_{drop}}{\pi \cdot \Delta x \cdot f(\theta)}} \tag{2}$$

The correction factor $f(\theta)$ can be determined from the height equation for a wetting drop of radius R_1 with a finite contact angle. Its height, h, is a function of the radial coordinate, r.

$$h(r) = \sqrt{\frac{{R_1}^2}{\sin^2\theta} - r^2} - \frac{R_1}{\tan\theta} \tag{3}$$

In eq 4, we calculate the actual cross-sectional area of the bead by integrating the height profile and then equate the resulting expression with a circular cross-sectional area times a correction factor. We can then solve for $f(\theta)$, which in our particular system (with a single contact angle) is a scalar number, approximately 0.852.

$$A_{\text{cross section}} = \int_{-R_1}^{R_1} \mathrm{d}r\, h(r) = \frac{1}{2}\pi {R_1}^2 f(\theta)$$

$$f(\theta) = \frac{2A_{\text{cross section}}}{\pi {R_1}^2} = \frac{2}{\pi}\left(\frac{\theta}{\sin^2\theta} - \cot\theta\right)$$

$$f(\theta = 82.7°) \cong 0.852 \tag{4}$$

Upon the basis of the observed radius of a falling drop, 28 μm, we find that each drop has a volume of about 90 pL. By examining the printed substrate, we find that the isolated drop radius, R_0, is 42.3 μm, which is larger than the 38.7 μm radius of a landed 90 pL drop with an 82.7° contact angle. Thus, a printed drop overexpands and remains pinned. (Its contact angle is a reduced 76.1°.) To account for this overexpansion, we define another accommodation factor in eq 5, $g(R_0)$, to link drop volume and substrate R_0. (We note that g depends on several factors, including drop fluid, momentum, and size, and whereas it remains constant for our experiment, we expect that it would vary in other situations). The g parameter allows us to scale distances in our calculations in terms of R_0, which is easily observed and relevant to the ultimate bead profile. For a 90 pL drop with a 42.3 μm landed radius, we find that g is about 0.568.

$$V_{drop} = \frac{2}{3}\pi {R_0}^3 g(R_0)$$

$$g(R_0) = \frac{V_{drop}}{\frac{2}{3}\pi {R_0}^3}$$

$$g(R_0 = 42.3\ \mu\text{m}) \cong 0.568 \tag{5}$$

To find a convenient dimensionless expression for a cylindrical bead radius, we scale R_1 from eq 2 by R_0 and introduce the dimensionless spacing $y \equiv \Delta x/R_0$ in eq 6. Substituting for drop volume from eq 5, we arrive at a convenient dimensionless expression for R_1/R_0. For the system under consideration, we plug our correction factors into this expression to yield the bead radius as a function of only y.

$$\frac{R_1}{R_0} = \sqrt{\frac{2V_{drop}}{\pi \cdot \Delta x \cdot f(\theta) \cdot {R_0}^2}}$$

$$\frac{R_1}{R_0} = \sqrt{\frac{2\left(\frac{2}{3}\pi {R_0}^3 g(R_0)\right)}{\pi \cdot \Delta x \cdot f(\theta) \cdot {R_0}^2}}$$

$$\frac{R_1}{R_0} = \sqrt{\frac{4}{3y}\frac{g(R_0)}{f(\theta)}} \cong \sqrt{\frac{0.888}{y}} \tag{6}$$

We would like to note that bead width as an inverse square of spacing is seen in recent efforts working from similar assumptions.[15,16] We present our derivation that emphasizes dimensionless spacing for clarity and completeness. The following work exploring the geometry of drop impingement and the implications on bead morphology is wholly unique.

Having determined the cylindrical bead radius as a function of drop spacing, we now consider the interaction between a landing drop and the already-formed uniform bead on the

(15) Stringer, J.; Derby, B. The Impact and Spreading of Ink Jet Printed Droplets. Organic Electronics Conference and Exhibition, Frankfurt, Germany; Sept 24-26, 2007.

(16) Smith, P. J.; Shin, D. Y.; Stringer, J. E.; Derby, B.; Reis, N. *J. Mater. Sci.* **2006**, *41*, 4153−4158.

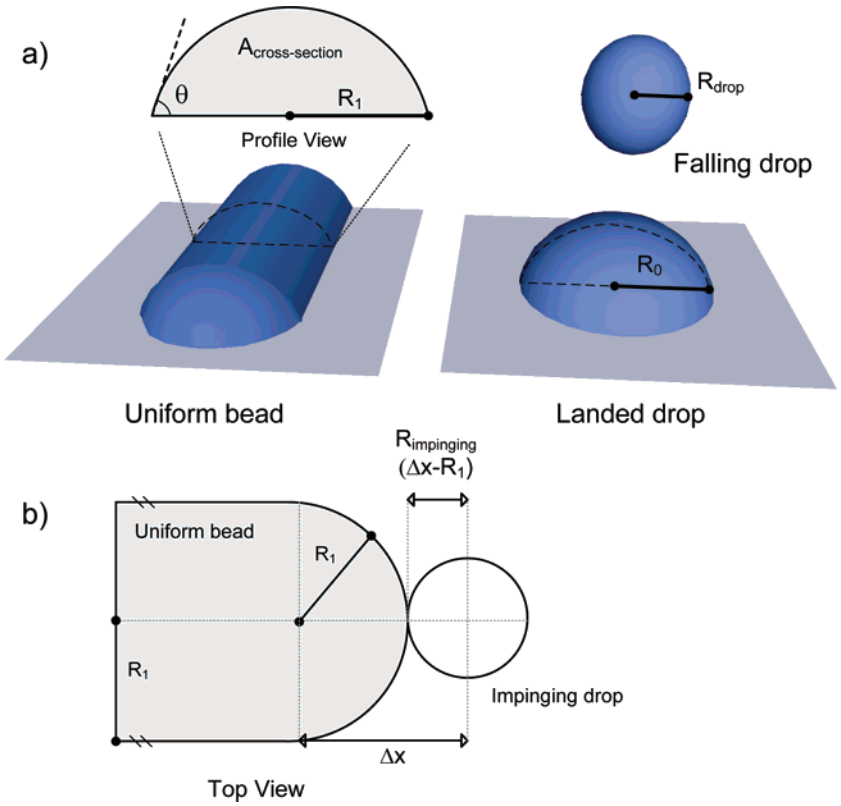

Figure 8. Geometry for the (a) uniform bead and landed drop and (b) impinging drop contact lines.

Table 1. Coffee Ring Factor for Uniform Lines and Individual Drops at Various Printing Temperatures

	coffee ring factor (peak/valley)	
temp (°C)	drop	line
17	ø	ø
30	1.03	ø
45	1.30	1.05
60	1.44	1.38

Table 2. Onset of Scalloping in Dimensionless Spacing at Each Print Temperature

temp (°C)	*y*
17	1.42
30	1.37
45	1.32
60	0.85

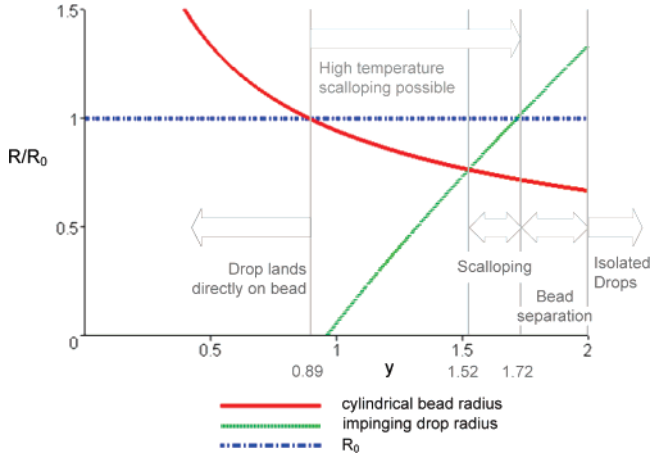

Figure 9. Nondimensional radius versus spacing.

substrate. We compare the energetics of drop spreading on a dry substrate to that of a drop spreading on an existing liquid film, the bead in our case. An outward-moving contact line of a drop on a dry substrate has been shown to be facilitated by a thin precursor film with a thickness on the order of angstroms. De Gennes showed that viscous energy dissipation during spreading is proportional to the fluid viscosity, η, times the logarithm of the spreading drop radius, R_0, divided the precursor film thickness, b.[17]

$$E \propto \eta \ln\left(\frac{R_0}{b}\right) \tag{7}$$

Should a liquid film be present, its thickness replaces the precursor film thickness. We expect that the wetted bead will have a thickness on the order of micrometers rather than the angstrom thickness of the precursor film. Thus, drop expansion into the bead will be energetically favorable by several hundred percent. An expanding drop in contact with a wetted bead and a dry substrate will flow preferentially into that bead.

Assuming that drops generally flow into the wetted bead when possible, we are now ready to consider the event of a drop landing as we increase the drop spacing. Figure 8b shows the contact line of a landing drop as it impinges upon a uniform bead. It is reasonable to assume a semicircular contact line at the end of a uniform bead to minimize curvature and thereby surface tension pressure. A new drop will land directly on the wetted bead first when Δx is less than R_1 (equivalently, $y < 0.89$), and the drop will flow into the existing bead rather than expand its contact line beyond that set by the advancing contact angle. The relevant spacing is shown in Figure 9 as the y where the cylindrical drop radius crosses 1.0, the isolated drop's radius. (All distances are dimensionless, scaled by R_0.)

When Δx is greater than R_1, or equivalently $y > 0.89$, a drop will first impact the substrate before its expanding contact line

(17) Degennes, P. G. *Rev. Mod. Phys.* **1985**, *57*, 827−863.

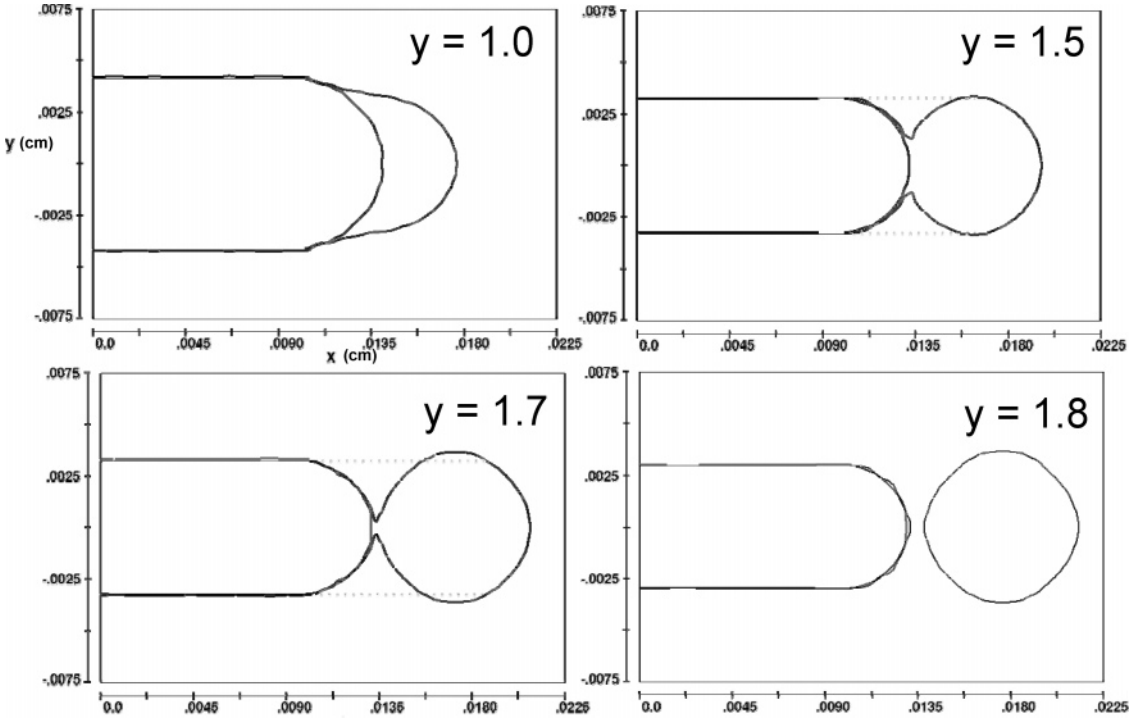

Figure 10. Simulated contact lines before and after the landing event, showing the initial pinned bead and the furthest extent of the contact line for noted dimensionless spacing y. A guide line is extended into the landing drop for clarity.

reaches the edge of the uniform bead. The radius of the new drop at impingement, $R_{\text{impinging}}$, will increase from zero at spacing $y = 0.89$ to R_0, the maximum size of an isolated drop near a spacing of $y = 2$. The geometry of the situation leads to the following expressions for the radius of an impinging drop. As in eq 6 above, we scale by R_0 to derive a dimensionless expression for $R_{\text{impinging}}$, which again becomes a function of only y in our system.

$$R_{\text{impinging}} = \Delta x - R_1$$

$$\frac{R_{\text{impinging}}}{R_0} = y - \sqrt{\frac{4}{3y}\frac{g(R_0)}{f(\theta)}} \cong y - \sqrt{\frac{0.888}{y}} \qquad (8)$$

Figure 9 also plots the impinging drop radius from eq 8.

Comparing R_1 and $R_{\text{impinging}}$, we see that the cylindrical bead has a larger radius from $y = 0.89$ to a spacing of about 1.52. If we assume that the impinging drop immediately ceases contact line expansion and preferentially flows into the cylindrical bead, then we would not expect to see scallops at spacings below $y = 1.52$ because each landing drop is not wider than the bead width when it encounters the bead.

Experimentally, we observe that at a given temperature and drop frequency the scallop behavior will begin at a certain drop spacing and become more pronounced as that spacing is increased until the drops completely separate at $y = 2$. At low temperature, 17 °C, scalloping begins around $y = 1.42$, similar to the 1.52 predicted above. At intermediate temperature, the onset of scalloping decreases to about 1.35, and at high temperature, we observe scalloping at $y < 1$. Table 2 shows the observed onset of scalloping at different temperatures.

One can make a qualitative argument regarding why scalloping occurs at decreasing y as temperature increases. At 17 °C, the time between landing drops is only about 1% of the drying time of a single drop, but at 60 °C, the time period between drops is 30% of an isolated drop's drying time. Thus at higher temperature, there is appreciable evaporation in the bead as printing proceeds. Not only is the bead thinner at high temperature but it is rapidly becoming more viscous as a result of gelation. (See Supporting Information: we measured a 2.4× increase in viscosity as the pedot concentration increases from 1.3% by weight to 2.0%.) Recalling eq 7, viscous energy dissipation during drop spreading is larger for the thinner, more viscous bead. Consequently, at higher temperature the bead is less able to channel drop expansion and arrest scalloping.

Returning to the examination of lines as we increase drop spacing, we consider the bead at the largest spacings, near $y = 2.0$. At $y > 1.72$, $R_{\text{impinging}}$ actually exceeds R_0 as shown in Figure 9. However, an impinging drop will not exceed its isolated drop radius. In other words, a falling drop will not interact with a cylindrically formed uniform bead above $y = 1.72$. Nevertheless, drops landing at y between 1.72 and 2.0 will impinge on one another if left unperturbed at their isolated radius, not forming a bead. (Circular drops overlap to $y = 2.0$.) This leads to the interesting contact line separation behavior in Figure 7c.

At y between 1.72 and 2.0, a second drop will impinge upon a landed circular drop with radius R_0 and flow into it as discussed above. Thus, it will not expand to its full isolated radius, and an elliptical contact line will form on the substrate. The next landing drop will not impinge upon this bead because it does not encounter the previous reflowed drop that did not fully expand to R_0. It will instead land and remain at the isolated drop radius until the next drop lands and wets it. This behavior will repeat in pairs indefinitely. As predicted, we see the onset of this contact line separation at $y = 1.72$ in our experimental data, and at 45 °C, we find optimal pairing around $y = 1.84$ (and similar behaviors at nearby spacings such as triples and alternating patterns; see Supporting Information for micrographs of many printed lines with spacings around $y = 1.72$).

To summarize, we used a simple model utilizing contact lines to explain the transition from a uniform bead to a scalloped contact line and eventually bead separation. At low spacing, where the next drop lands directly on the bead, no scalloping takes place. At sufficient spacing, the drop lands on the bare substrate first, and its contact line expands from a point as a

circle of growing radius. When the expanding drop diameter at bead impingement exceeds the bead width, scalloping occurs. Because the impinging drop radius exceeds the equilibrium bead radius at large spacings (nearly the drop diameter), drops may impinge upon a previous drop but not a formed bead. Paired groups and similar breakup phenomena result.

Whereas the above discussion, based upon the meeting of contact lines, proves effective for predicting the line morphology as we vary drop spacing, it is not always useful in predicting outcomes, including line width where several forces are in competition. For example, at larger spacings before the onset of scalloping (ca. $y = 1.4$), the spreading momentum of the falling drop on a dry substrate competes with the flow into the bead once contact is made. Both effects compete, and an intermediate line width results (though the contact line does remain uniform). The interplay of these forces indicates that more sophisticated modeling would be useful for more precise predictions.

To corroborate the simple impingement flow model developed above and as an aid to visualization, we simulated the drop−landing−impinging event using commercial computational fluid dynamics software, Flow3D. It solves the 3D Navier−Stokes and mass continuity equations for a predetermined mesh using a finite difference approximation with the volume-of-fluid method. The fluid is treated as a non-Newtonian, incompressible fluid with a sharply defined free surface. (In the volume-of-fluid method, the free interface is inferred from the fluid fraction of each grid cell. Because each cell can contain at most one free-surface interface, the grid resolution, a 3 μm cube in our case, determines when two free surfaces approaching one another are merged.) Heat transfer and phase change are not included for the relatively brief event of drop impingement. The landing drop has an 82.7° contact angle with an impermeable planar substrate, and the preexisting bead has a pinned contact line that sets its initial contact angle to 82.7°. A no-slip condition is imposed on fluid in contact with the substrate.

We simulated a 90 pL drop landing at 1 m/s upon a substrate with an appropriately sized uniform bead. Figure 10 shows the contacts lines before and after the landing event at four different spacings. The inner line shows the initialized, pinned bead before the drop lands, and the outer line represents the maximum extent of contact line expansion following drop impact. Also, guide lines are extended from the uniform bead to help show where scalloping is occurring. As we see in Figure 10a, no expansion past the uniform width is seen when the drop lands directly on the bead at $y = 1$. At $y = 1.5$, we see that the drop expands to equal the bead width, and at greater y, the landing drop expands past the edge of the bead. The bead separates by $y = 1.8$. This matches our empirical results and also the simple geometrical model proposed above. See Supporting Information for 3D animations of the drop landing event at each spacing.

6. Conclusions

We studied inkjet-printed features of PEDOT/PSS. We considered different printed line topologies as they occur throughout the experimental space. At high temperatures and/or large delays between individual drops, stacked coin behavior is seen as each drop individually dries. At small spacings and lower temperatures, periodic overflow of a uniform bead is seen as fluid in the bead exceeds the equilibrium contact angle of the system. At intermediate spacings and temperature, a uniform bead can be printed. If the drop spacing is increased too far, then the uniform bead forms scallops before the bead begins to separate and isolated drops will land and dry.

For printed wires, two of these morphologies are appropriate. As we saw in Figure 1, wires in printed circuits have typically been printed as stacked coins. This results in reproducible features that are appropriate for interconnecting wires or a printed inductor. At high temperature, these predictable features can be printed quickly. However, for other electronic devices including transistors and capacitors the uneven line surface and edge will lead to a loss of control over properties such as the dielectric thickness and channel length. Therefore, printing a uniform bead with a controlled coffee ring is appropriate even if there is a tradeoff in fabrication speed.

By controlling the substrate temperature beneath the drying feature, we demonstrated control of its topology, reversing or enhancing the coffee ring effect. A heated substrate leads to greater evaporation at the bead's edge, which then yields an enhanced coffee ring, compared to room-temperature drying. Analogously, a cooled substrate suppresses edge evaporation and eliminates the coffee ring at the feature's edge. These effects occur more strongly in a circular drop than in a straight line because of the greater ratio of edge length to center area in the drop. Tuning the radial distribution of solute in a drying drop suggests applications beyond printed electronics, for instance, calibrated microlenses.

Having studied the properties of this particular ink−substrate system in detail, we can enumerate the features that lead to a narrow, uniform bead. Contact line pinning is essential; it permits the adjustment of the evaporation profile to create a desired feature shape. It also provides stability to the wetted bead to prevent it from moving and separating, as would occur with detached drops. Also, a large wetting contact angle (approaching, but not larger than, 90°) leads to better results. Small contact angle systems are more susceptible to forming coffee rings because of their greater volume of fluid in proximity to the contact line, and for a given volume drop, they will have a wider line. Finally, if the above conditions have been met, an absence of Marangoni flows allows control of a single solvent system. The development of a higher-conductivity ink that meets these conditions would be useful to furthering the development of printed electronics because pedot falls many orders of magnitude shy of the conductivity of a good metal.

Acknowledgment. We owe our gratitude to Professor Stephen Morris for his gracious, patient advice. The National Science Foundation Graduate Research Fellowship supported this work, and a portion of this work was supported by the Director, Office of Science, Office of Basic Energy Sciences, Division of Materials Sciences and Engineering, of the U.S. Department of Energy under contract DE-AC03-76SF00098.

Supporting Information Available: Fluid properties of pedot ink. Micrographs of printed lines near the separation spacing. Animation of CFD results showing droplet impingement at several spacings. This material is available free of charge via the Internet at http://pubs.acs.org.

LA7026847